OPTICAL STUDIES OF SHEARED POLYMER DROPLETS

Erik K. Hobbie and Kalman B. Migler
National Institute of Standards and Technology
Gaithersburg, Maryland

Abstract

The use of shear flow to emulsify immiscible polymers is ubiquitous in the processing of polymer blends. Although the pioneering work of Taylor [1-4] on isolated Newtonian droplets remains at the foundation of our understanding, emulsions of viscoelastic fluids can display a variety of interesting and novel phenomena under shear [5-9]. Here, video microscopy is used to measure the shear response of dilute polymeric emulsions. At low shear rates, the behavior is in agreement with the Taylor picture. In the limit of strong shear, we observe a transition in which the droplets elongate along the vorticity axis. A simple model is offered that relates this behavior to the viscoelastic nature of the melt components.

Background

The details of the instrument are described elsewhere [10]. By machining optical windows into a narrow channel attached to the end of a twin-screw extruder, we can observe blends of viscous polymer melts at shear rates where normal stresses in the melt components are comparable to or greater than the shear stress. A schematic of the experiment is shown in Fig. 1. For a pressure-driven flow, the effective shear rate ($\dot{\gamma}$) of a *locally* simple shear flow is a function of the distance from one of the walls, and we describe measurements made at the surface of the bottom window [11].

The materials (provided by DOW[*]) are polystyrene (PS) and polyethylene (PE) at T = 195 ^{o}C. The molecular weights[**] of the four components are M_w = 195k (M_n = 83k) for PS_1, M_w = 342k (M_n = 141k) for PS_2, M_w = 85.2k (M_n = 15.4k) for PE_1, and M_w = 83.1k (M_n = 25.6k) for PE_2, where PE_1 is low-density with long-chain branching and PE_2 is linear high-density. The melt rheology at 195 ^{o}C was measured in a parallel-plate rheometer [12]. All the components exhibit (Fig. 2) a low-$\dot{\gamma}$ plateau in the steady-shear viscosity that crosses over to shear thinning behavior at modest $\dot{\gamma}$. We describe data from 1% (mass fraction) blends of PS_1 in PE_1, PS_1 in PE_2, and PS_2 in PE_1.

Results

We observe a variety of droplet shapes as a function of $\dot{\gamma}$ and the viscosity ratio λ. For PS_2 in PE_1 spherical droplets are elongated along $\hat{\mathbf{x}}$ into elliptical shapes that develop a cusp-like crease in the equatorial x-y plane at high $\dot{\gamma}$. For PS_1 in PE_1, similarly shaped droplets exhibit a transition in which they become modestly extended along $\hat{\mathbf{z}}$ at high $\dot{\gamma}$. For PS_1 in PE_2 (Fig. 3), spherical domains are first pulled into thin filaments along $\hat{\mathbf{x}}$ that then exhibit a transition to worm-like shapes extended along $\hat{\mathbf{z}}$ at high $\dot{\gamma}$.

At the highest flow rates, we estimate the Reynolds number (*Re*) to be less than 10^{-3}. In the low-*Re* theory of Taylor [1,3], the steady-state shape of an initially spherical droplet (radius R_o) can be calculated by balancing the shear stress with the restoring force due to surface tension, which yields an ellipsoid of major axis L = $R_o(1 + D)$ and minor axis B = $R_o(1 - D)$, oriented in the x-y plane with long axis at 45 degrees to the flow direction, undistorted in the $\hat{\mathbf{z}}$ (vorticity) direction. The quantity D = (L - B)/(L + B) = $f(\lambda)$Ca, where $f(\lambda)$ is a constant of order unity, gives the deformation in terms of the capillary number $\mathrm{Ca} = \eta R_o \dot{\gamma} / \sigma$, where σ is the interfacial tension [1,3].

We consider ensemble averages of $D_{xz} = (R_x - R_z)/(R_x + R_z)$ as a function of $\dot{\gamma}$ for each of the mixtures. A collection of droplets elongated along $\hat{\mathbf{x}}$ will then have $\langle D_{xz} \rangle > 0$, while droplets elongated along $\hat{\mathbf{z}}$ will have $\langle D_{xz} \rangle < 0$, and this quantity thus provides a measure of both the orientation and magnitude of the deformation, with $-1 < \langle D_{xz} \rangle < 1$. The results are shown in Fig. 4. All of the mixtures show an initially linear increase (inset) that levels off at moderate $\dot{\gamma}$ and then starts to decrease. For PS_1/PE_1 and PS_1/PE_2, $\langle D_{xz} \rangle$ becomes negative in the limit of strong shear. The transition region corresponds to a coexistence of the two orientations. In the weak-shear regime, the estimate $\sigma \sim 10$ mN/m follows from a linear fit of the data (inset Fig. 4) via the Taylor theory, in order-of-magnitude agreement with the quoted value of 5.6 mN/m [13].

By considering a stress balance at the droplet interface, one can argue [14] that a qualitative condition for the vorticity elongation of polymer droplets under shear in a polymer matrix is $\delta N_1 = (N_1)_{PS} - (N_1)_{PE} > 0$, where N_1 is the first normal stress difference. The parallel-plate rheometer [12] measures $N_1 - N_2 \sim N_1$ (using the approximation $N_2 \sim N_2$), and we plot this quantity as a function of the shear stress in each of the pure melt components for each of the three blend pairs (Fig. 5). At the shear rates (stresses) accessible to the parallel plate rheometer, $\delta N_1 < 0$. However, extrapolation

of the normal stress data to higher shear stresses (Fig. 5) yields a transition to $\delta N_1 > 0$ at *roughly* 65 kPa for $\lambda = 22$ and 45 kPa for $\lambda = 1.8$, corresponding to shear rates of 10^3 1/s and 2 x 10^2 1/s, respectively, in qualitative agreement with Fig. 4. The $\lambda = 240$ blend exhibits either vorticity elongation nor an extrapolated crossover in the normal stress difference.

Conclusions

Physically, we suggest the following qualitative picture of the transition to vorticity elongation in the system under consideration. At low $\dot{\gamma}$, droplets are elongated along the flow direction due to the dominance of shear forces. At high $\dot{\gamma}$, normal stress differences become larger than the shear stress, with vorticity elongation emerging when $\delta N_1 > 0$. The results suggest that normal forces can have profound effects on the morphology of multi-phase polymeric materials under realistic processing conditions.

References

* Certain materials are identified in order to adequately specify the experimental conditions. Such identification does not imply recommendation by NIST, nor does it imply that the materials are the best available for the purpose.

** According to ISO 31-8, the term "molecular weight" has been replaced by "relative molar mass" denoted by M_r. The conventional notation rather than the ISO notation has been used in this publication. Error bars, which unless otherwise specified are the size of the data markers, represent the best estimate of 2 standard deviations in the total experimental uncertainty.

1. G. I. Taylor, *Proc. R. Soc.* **A138**, 41 (1932); *Proc. R. Soc.* **A146**, 501 (1934).

2. B. J. Bentley and L. G. Leal, *J. Fluid Mech.* **167**, 241 (1986).

3. J. M. Rallison, *Ann. Rev. Fluid Mech.* **16**, 45 (1984).

4. S. Torza, R. G. Cox, S. G. Mason, *J. Coll. Interface Sci.* **38**, 395 (1972); F. D. Rumscheidt and S. G. Mason, *J. Coll. Sci.* **16**, 238 (1961).

5. E. Bartram, H. L. Goldsmith, and S. G. Mason, *Rheol. Acta* **14**, 776 (1975).

6. H. J. Van Oene, *J. Coll. Interface Sci.* **40**, 448 (1972).

7. J. J. Elmendorp and R. J. Maalcke, *Polym. Eng. Sci.* **25**, 1041 (1985).

8. P. P. Varanasi, M. E. Ryan, and P. Stroeve, *Ind. Eng. Chem. Res.* **33**, 1858 (1994).

9. L. Levitt, C. W. Macosko, and S. D. Pearson, *Polym. Eng. Sci.* **36**, 1647 (1996).

10. S Li, K. Migler, E. Hobbie, H. Kramer, C. Han, and E. Amis, *J. Polym. Sci., Polym. Phys.* **35**, 2935 (1997).

11. The shear rate at the wall can be determined in two ways. Particle-tracking-velocimetry [10] measures the velocity gradient at the bottom window, from which we get $\dot{\gamma}$. Treating the slit die as a capillary rheometer [C. W. Macosko, *Rheology; Principles, Measurements, and Applications* (VCH, New York, 1994).] we compute $\dot{\gamma}$ at the wall from measurements of the volumetric flow rate and pressure drop through the channel. For PE_2 melts, the values determined with these two methods are in reasonable agreement, and here we opt for the latter as it is less labor intensive.

12. For the parallel-plate geometry, measurements of the torque and normal force have been corrected [see, for example, R. B. Bird, R. C. Armstrong, and O. Hassager, *Dynamics of Polymeric Liquids, Vol. 1* (Wiley, New York, 1987)] to obtain the shear viscosity, η, and normal stress difference, $N_1 - N_2$, as a function of $\dot{\gamma}$.

13. N. Mekhilef, B. D. Favis, and P. J. Carreau, *J. Polym. Sci., Polym. Phys. Ed.* **35**, 293 (1997).

14. E. K. Hobbie and K. B. Migler, to be published.

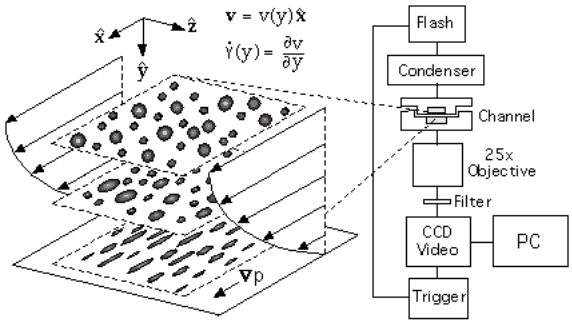

Fig. 1-Schematic of the experiment.

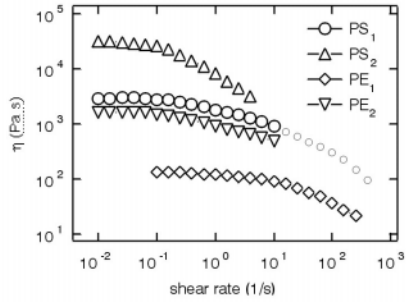

Fig. 2-Shear viscosity of the pure melt components at 195 °C

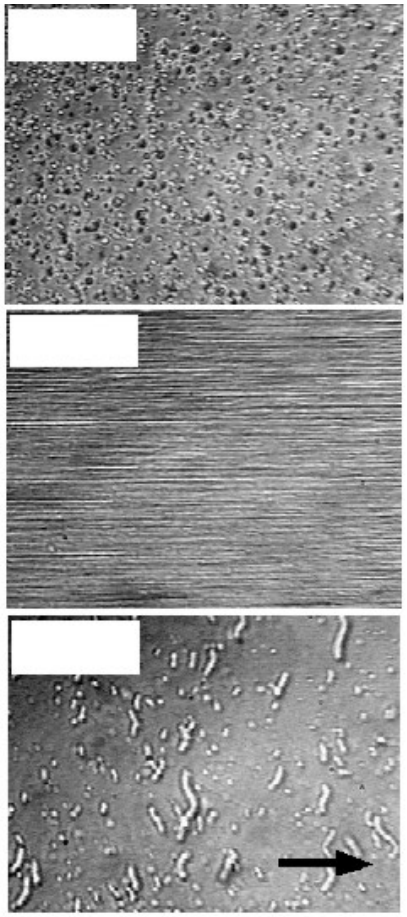

Fig. 3-Droplet morphology as a function of shear rate for 1% PS_1 in PE_2 at 195 ^{0}C. The width of each micrograph is 200 μm, with the flow direction from left to right and the vorticity direction from top to bottom.

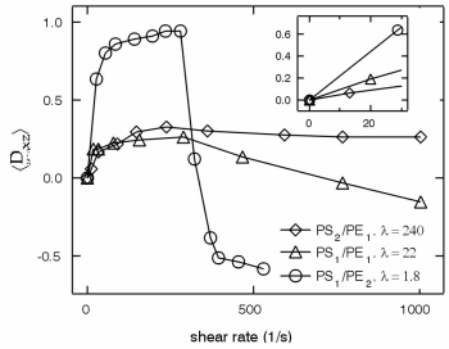

Fig. 4-Average deformation number (in flow-vorticity plane) vs. shear rate at 195 °C.

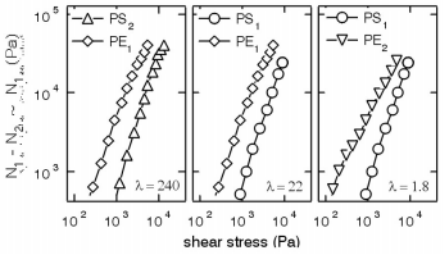

Fig. 5-First normal stress difference vs. shear stress in the melt components at 195 °C.